Experimental Investigation of Core-Valence Double Photoionization

Y. Hikosaka,[1] T. Aoto,[2] P. Lablanquie,[3] F. Penent,[3] E. Shigemasa,[1] and K. Ito[2]

[1]*UVSOR Facility, Institute for Molecular Science, Okazaki 444-8585, Japan*

[2]*Photon Factory, Institute of Materials Structure Science, Oho, Tsukuba 305-0801, Japan*

[3]*LCP-MR, Université Pierre et Marie Curie Paris 6 and CNRS (UMR 7614), 11 rue Pierre et Marie Curie, 75231 Paris Cedex 05, France*

(Received 16 May 2006; published 3 August 2006)

Core-valence double photoionization has been observed in Ne atoms and N_2 molecules using a magnetic-bottle time of flight spectrometer. The multielectron coincidence data sets give complete information on the energy correlations between all emitted electrons, which supports a detailed description of the core-valence double photoionization processes including direct spectroscopy of the core-valence doubly ionized states, the final states populated by their Auger decay and details of the dynamics of core-valence double photoionization for selected states.

DOI: 10.1103/PhysRevLett.97.053003 PACS numbers: 32.80.Fb, 32.80.Hd, 33.15.Ry, 33.60.Fy

The double photoionization (DPI) of atoms and molecules has attracted special attention for a long time because this process is due entirely to electron correlation, and, consequently, investigations of DPI reveal fundamental aspects of atomic and molecular physics. The shake theory [1] provides a basic understanding of DPI: The sudden change of the nuclear charge during single photoionization ejects another electron into a continuum state (shakeoff). While the sudden approximation describes the situation in the high-energy limit, the description for DPI processes at finite energies is still the subject of discussion [2].

Until now, most DPI studies have concentrated on the removal of two valence electrons. Direct experimental observations of core-valence DPI are limited to a few cases involving, for example, the $2p$ core hole in Na [3] or the $4d$ hole in Xe [4]. Theoretical calculations have identified peculiar properties of core-valence doubly ionized states [5]. The formation of such states has been known since the introduction of x-ray photoelectron spectroscopy. In inner-shell photoelectron spectra [6], they contribute to the background enhancements lying at the converging limits of photoionization satellite states. However, investigations using conventional photoelectron spectroscopy offer neither direct spectroscopy of the doubly ionized states nor the detailed DPI dynamics. In contrast, coincidence detection between the two photoelectrons emitted in DPI processes provides direct spectroscopic information on DPI processes. A sophisticated coincidence method is required, because the DPI cross section is unfavorable as compared with the main inner-shell ionization processes, and, consequently, the events associated with these DPI processes are easily hidden behind ordinary inner-shell photoionization events.

In this Letter, we present an investigation of DPI associated with the removal of a $1s$ electron in Ne and in N_2 using a very efficient coincidence technique. We have used a magnetic-bottle time of flight (TOF) electron spectrometer for which the powerful capabilities of electron coincidence observations have recently been described [7,8]. The coincidence data sets accumulated include and reveal complete information on the energy correlations between all the electrons emitted, from which novel and exhaustive knowledge of the DPI process can be deduced.

The experiments were performed on the beam line AR-NE1B of the PF-AR storage ring specifically dedicated to single bunch operation. The 377-m circumference of the storage ring provides a 1.26-μs repetition period for the 100-ps-width light pulses. The light emitted in a helical undulator is monochromatized by a vertical-dispersion spherical-grating monochromator, and the photon energy resolution is set to <1 eV (FWHM). A gas beam effusing from a 500-μm inner-diameter needle crosses the monochromatized light beam at a right angle. Multicoincidences between electrons which are analyzed in energy by their TOF in the magnetic-bottle electron spectrometer are recorded and analyzed. The analyzer used in the present experiments is similar to that developed by Eland *et al.* [7], except for the shorter 2.5-m flight length in the present analyzer instead of the original 5-m length. A strong permanent magnet (NdBFe: $\sim$0.7 T) located close to the interaction region creates, with the inhomogeneous magnetic field, a magnetic mirror for electrons that are hence guided by the weak magnetic field ($\sim$1 mT) of a long solenoid toward a position sensitive detector composed of two microchannel plates in chevron followed by a phosphor screen. Signals from the detector are fed into a multistart (common-stop) time-to-digital converter (RoentDek TDC8). The converter is triggered by the arrival of a first electron and is stopped, after a 15-μs delay, by the ring clock signal. All of the electrons arriving in this time window are detected. Their absolute TOF is then recalculated with respect to the ring clock. The absolute electron TOF, the energy resolution, and the detection efficiency were calibrated by measuring Ne $1s$ photoelectrons at different photon energies. For electrons having less than 300 eV kinetic energy, the energy resolving power of the apparatus $E/\Delta E$ is nearly constant at 30. The detection efficiency is also constant for electrons of less than 200 eV but drops gradually above 200 eV.

A multielectron coincidence data set for Ne was accumulated at an excess energy of 108.7 eV above the Ne $1s$ ionization threshold at 870.09 eV [9]. Figure 1(a) shows the photoelectron spectrum, where the energy range is adjusted to show the photoelectron peaks for formation of the $Ne^+ 1s^{-1}$ state and of the satellite states. The satellite states $Ne^+ 1s^{-1}2p^{-1}(^{1,3}P)np$ [10] are resolved only partially with an instrumental resolution of about 3 eV. Figure 1(b) displays a two-dimensional (2D) map showing the coincidences between the photoelectrons and slower electrons in the 0–30 eV energy range.

On this 2D map, a vertical stripe appears at the fast electron energy corresponding to the $1s$ photoelectrons. These slow electrons are produced through the Auger decay of the $1s$ core hole: The coincidences occur between the $1s$ photoelectron and slower Auger electrons produced in the double Auger decay. The yield along this vertical stripe shows a steep decrease as the energy of the slow electron increases. This is reasonable, considering the energy sharing of the two Auger electrons in the double Auger decay [11]. In contrast, knots of enhancements at given energies are observed along the vertical stripes corresponding to the satellite photoelectrons. They are assigned mainly to cascade Auger decays from the satellite states [12]. In a simple spectator model, the $Ne^+ 1s^{-1}2p^{-1}(^{1,3}P)np$ satellite states undergo an Auger decay towards excited Ne^{2+} states with configurations such as $2p^{-3}np$ and $2s^{-1}2p^{-2}np$. If these excited states lie above the Ne^{3+} threshold, they autoionize and produce the low-energy electrons observed in the 2D spectrum [12].

Two intense diagonal stripes are observed in the fast electron energy range of 30–60 eV on the 2D map. They are due to coincidences between two photoelectrons emitted through the formation by DPI of the $Ne^{2+} 1s^{-1}2p^{-1}(^{1,3}P)$ states. The available energy to form each Ne^{2+} state, given by (photon energy)-(binding energy of the Ne^{2+} state), is shared by the two photoelectrons emitted if we neglect the postcollision interaction (PCI) due to the subsequent Auger decay of the Ne^{2+} states with a remaining $1s$ vacancy. This PCI is expected to affect essentially low-energy photoelectrons and, hence, to cause distortion from a straight line. Such an effect cannot be observed in Fig. 1(b), suggesting that PCI effects can be ignored here within our limited experimental resolution. It may be possible to observe this distortion at a lower excess energy close to the threshold.

To reveal the Ne^{2+} states with a $1s$ core hole more clearly, the coincidence counts on the 2D map are integrated and projected on the diagonal axis $X = Y$ in order to present the sum of the energies of fast and slow electrons for all coincident events. This projection is represented as a function of the total energy of the two electrons in Fig. 2. The high statistics arising from the integration enables us to find, as well as the $1s^{-1}2p^{-1}$ peaks, two weak peaks associated with the $1s^{-1}2s^{-1}$ states that are faintly visible on the 2D map. Although the background underlying the peaks must include true coincidences between two slow Auger electrons in the triple Auger decay of $1s^{-1}$, false coincidences are the main contribution to the background. Until now, the energy levels of the Ne^{2+} states with a $1s$ core hole have been estimated from the extrapolation of the converging limits of the $1s$ satellite states [10] or from x-ray fluorescence energies [13]. The present spectrum

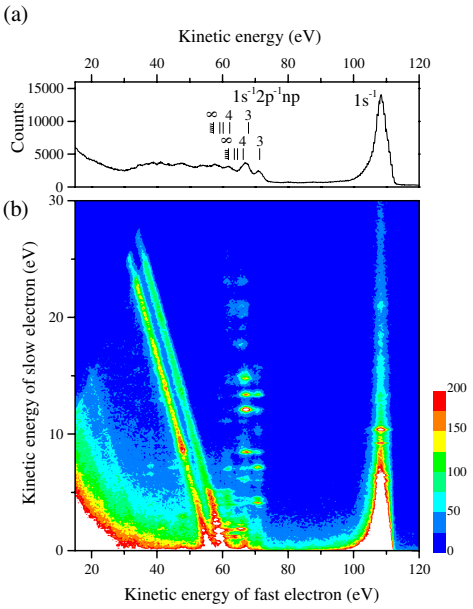

FIG. 1 (color online). (a) Inner-shell photoelectron spectrum of Ne obtained at the photon energy of 978.8 eV. (b) Two-dimensional map of all coincidence pairs, represented as a function of the kinetic energies of fast and slow electrons. Coincidence intensities in the two-dimensional map are plotted on a linear scale. In (a), the positions of the photoionization satellites converging to the Ne^{2+} $1s^{-1}2p^{-1}(^{1,3}P)$ states are extracted from Ref. [10].

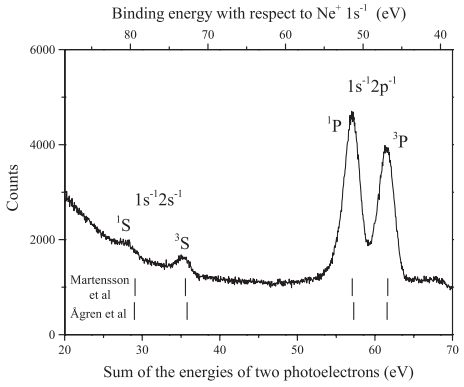

FIG. 2. Histogram of the kinetic energy sum for two electrons detected in coincidence, as deduced from Fig. 1(b) by integrating the yields along the direction for (fast electron energy) + (slow electron energy) = constant. The top axis gives the binding energies of the core-valence doubly ionized Ne^{2+} states with respect to the Ne^+ $1s^{-1}$ state, where it is assumed that the kinetic energy shifts due to the postcollision interaction are negligible. Binding energies from Refs. [10,13] are indicated.

allows us to locate directly the Ne^{2+} states since the incident photon energy is known. The binding energies of the Ne^{2+} states with respect to Ne^+ $1s^{-1}$, thus obtained and shown in Fig. 2, agree within 0.2 eV with the previous estimations [10,13], except for the $1s^{-1}2s^{-1}(^1S)$ state.

The intensity ratio of the ^3P, ^1P, ^3S, and ^1S peaks in Fig. 2 is 1:1.34:0.12:0.05. The ratio of the ^3P and ^1P peaks differs significantly from the statistical value $^3P/^1P = 3$. The $^3P/^1P$ intensity ratio has been studied by high-energy electron impact, and a value $^3P/^1P = 1.8 - 2$ was deduced [13–15]. The discrepancy between the ratios obtained by electron impact and the statistical value was explained in terms of the continuum mixing within the framework of the shake model [16]. The present $^3P/^1P$ ratio 0.74 is much smaller than the values observed by electron impact. This suggests the breakdown of the sudden approximation near the DPI thresholds. The ratio $(^3P + ^1P)/(^3S/^1S) = 13.8$ is much bigger than both the corresponding ratios determined by electron impact ionization (4.7 [13]) and deduced from a theoretical calculation (9.1 [17]). This could also result from the DPI dynamics at the threshold region.

In order to study how the two photoelectrons produced from the DPI processes in Ne share the available energy, we have extracted the intensity distributions along the two intense diagonal stripes in Fig. 1(b) and plotted them in Fig. 3. Resonance structures are discernible on both distributions corresponding to the $1s^{-1}2p^{-1}$ DPI continua. The resonance structures below 5 eV in the ^3P continuum are attributed to autoionization from the $Ne^+ 1s^{-1}2p^{-1}(^1P)np$ states. The other resonances in the two curves can be assigned to the satellite states Ne^+ $1s^{-1}2s^{-1}(^{1,3}S)ns$, from their known binding energies [10]. Some resonances of Ne^+ $1s^{-1}2s^{-1}(^{1,3}S)ns$ are apparently asymmetric, which results from interactions and interference with the DPI continua in which they are embedded.

The photoionization satellite states Ne^+ $1s^{-1}2s^{-1}(^{1,3}S)ns$ also exhibit asymmetric peak shapes in conventional photoelectron spectra [10,18,19]. The peak shape of the Ne^+ $1s^{-1}2s^{-1}(^3S)3s$ resonance isolated in the photoelectron spectra has been studied theoretically [20,21] as a prototype of resonances embedded in DPI continuum associated with core-hole creation. The asymmetry observed by conventional photoelectron spectroscopy results from interactions with the two possible continua for the formation of the Ne^{2+} $1s^{-1}2p^{-1}(^{1,3}P)$ states. In contrast, each curve in Fig. 3 exhibits the asymmetry resulting from the interaction with the corresponding continuum, which enables us to inspect more precisely the coupling of the discrete state with each continuum. The asymmetric peaks for the Ne^+ $1s^{-1}2s^{-1}(^3S)3s$ state are fitted by a convolution of the Fano profile [22] with a triangular instrumental profile [23]. The Fano q parameters are thus found to be 4.1 ± 0.4 and 1.0 ± 0.1 for the Ne^+ $1s^{-1}2s^{-1}(^3S)3s$ resonance state in the ^1P and ^3P continua, respectively. Here the natural width of the state has been

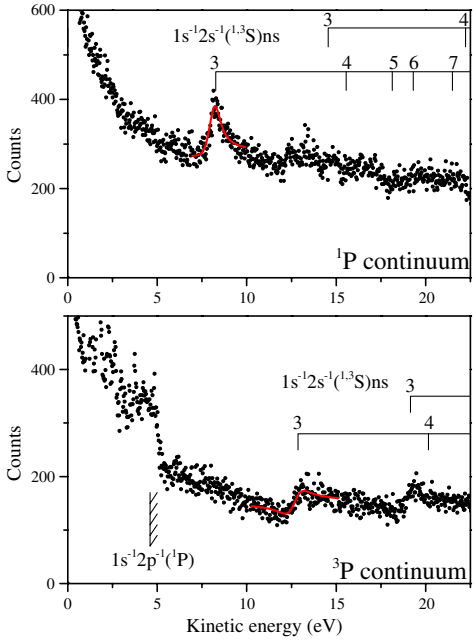

FIG. 3 (color online). Kinetic energy distributions of photoelectrons associated with the formations of Ne^{2+} $1s^{-1}2p^{-1}(^{1,3}P)$. They have been obtained by plotting intensities along the corresponding diagonal stripes in the two-dimensional coincidence map of Fig. 1(b). The integration ranges selected for the $1s^{-1}2p^{-1}(^3P)$ and $1s^{-1}2p^{-1}(^1P)$ continua correspond, respectively, to 60.6–63.8 and 54.0–58.1 eV in Fig. 2. The locations of the Ne^+ $1s^{-1}2s^{-1}(^{1,3}S)ns$ states are determined from the reported energy levels [10]. The $1s^{-1}2s^{-1}(^3S)3s$ peaks are fitted by a convolution of the Fano formula [22] with a triangular instrumental profile [23].

fixed at the reported value of 0.57 eV [18]. The present q values should be valuable in validating the theoretical frameworks of the available calculations.

The Ne^{2+} ions formed after core-valence DPI can undergo nonradiative decay producing fast Auger electrons. In practice, we can also detect these fast Auger electrons in coincidence with the two photoelectrons (triple coincidences) even if the detection efficiency and the energy resolution for such energetic (about 800 eV) electrons is limited. The energy distribution of the fast Auger electrons in these triple coincidences is compared in Fig. 4 with the Auger spectrum associated with the Ne^+ $1s^{-1}$ state. As the Auger energies correspond to the energy differences between the initial core-hole states and Auger final states, the Auger spectra have been scaled to reveal the binding energies of the final states. The Auger electron distribution from the Ne^+ $1s^{-1}$ state is interpreted as forming mainly the Ne^{2+} $2p^{-2}$ and $2s^{-1}2p^{-1}$ states lying in the ionization energy range of 62–98 eV [24]. Note that the energy resolution for the fast Auger electrons is only 20–30 eV (FWHM). Meanwhile, the Auger electron distribution from the Ne^{2+} $1s^{-1}2p^{-1}$ state shows that the population of the Auger final states shifts towards higher binding energy. The onset of the Auger distribution agrees

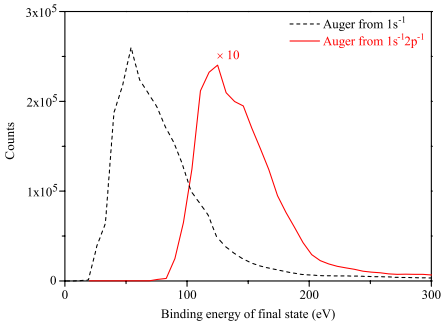

FIG. 4 (color online). Auger electron spectra measured in coincidence with the photoelectrons for the formations of the $1s^{-1}$ (dashed black line) and $1s^{-1}2p^{-1}$ states (solid red line). The spectra are plotted as a function of the binding energies of the final states after Auger decay, which are, respectively, Ne^{2+} or Ne^{3+} states. Binding energies are referenced to the Ne neutral ground state.

reasonably with the lowest ionization energy for formation of the Ne^{3+} state at 125.951 eV [24].

The present coincidence method reveals its spectroscopic usefulness even more strikingly when applied to molecules. This is because spectroscopic information on molecular doubly charged ionic states with a core hole is extremely rare. Figure 5 shows the coincidence spectra for N_2 obtained with the same procedure as for Fig. 2. The structures correspond to core-valence doubly ionized states. The equivalent core model which assimilates N_2^+ $1s^{-1}$ and NO^+ $2\pi^{-1}$ can be used to estimate binding energies of the N_2^{2+} $1s^{-1}v^{-1}$ states from those of the NO^{2+} $2\pi^{-1}v^{-1}$ states, and the binding energies estimated for N_2^{2+} $1s^{-1}v^{-1}$, with $v = 3\sigma_g$, $1\pi_u$, and $2\sigma_u$, correspond roughly to the three broad bands observed. Recent calculations [5] predict strong state dependent singlet-triplet splittings which are in remarkable agreement with our experiment, considering its limited energy resolution.

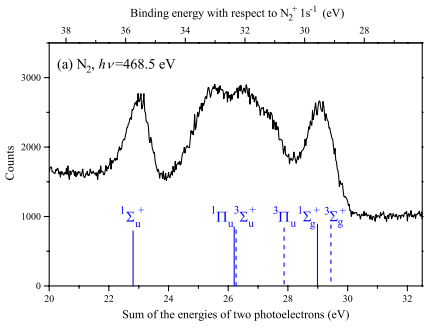

FIG. 5 (color online). Histogram of the kinetic energy sum for two photoelectrons detected in coincidence, measured in N_2 at the photon energy of 468.5 eV. The spectrum exhibits N_2^{2+} $1s^{-1}v^{-1}$ states. The top axis gives their binding energies with respect to the N_2^+ $1s^{-1}$ state which was taken at 409.94 eV [25]. Bars present the configuration interaction calculations from Ref. [5]. The N_2^{2+} $1s^{-1}v^{-1}$ states are split into the singlet and triplet components, represented with a solid line and dotted lines, respectively.

However, further high resolution experiments are needed to definitively identify the three structured features on the central band.

In conclusion, we have studied the core-valence DPI process in Ne and N_2 with a multielectron coincidence method. The magnetic-bottle TOF spectrometer allows such studies to be carried out with very high efficiency. The present work gives exhaustive information on the DPI processes involving core electrons. Moreover, this work demonstrates the high performances of the multielectron coincidence method both for DPI dynamics in the inner-shell range and for the spectroscopy of the associated doubly charged ions.

We thank S. Carniato for fruitful discussions and G. Stark for critical reading. We are grateful to the Photon Factory staff for the stable operation of the PF-AR. This work was performed under the approval of the Photon Factory Advisory Committee (Proposal No. 2004G210).

[1] T. Åberg, Phys. Rev. **156**, 35 (1967).
[2] T. Pattard, T. Schneider, and J. M. Rost, J. Phys. B **36**, L189 (2003).
[3] F. Wuilleumier *et al.*, Phys. Rev. Lett. **73**, 3074 (1994).
[4] P. Bolognesi *et al.*, Phys. Rev. A **64**, 012701 (2001).
[5] H. Schulte *et al.*, J. Chem. Phys. **105**, 11 108 (1996).
[6] K. Siegbahn *et al.*, *ESCA Applied to Free Molecules* (North-Holland, Amsterdam, 1969).
[7] J. H. D. Eland *et al.*, Phys. Rev. Lett. **90**, 053003 (2003).
[8] F. Penent *et al.*, Phys. Rev. Lett. **95**, 083002 (2005).
[9] A. P. Hitchcock and C. E. Brion, J. Phys. B **13**, 3269 (1980).
[10] N. Mårtensson, S. Svensson, and U. Gelius, J. Phys. B **20**, 6243 (1987).
[11] J. Viefhaus *et al.*, J. Electron Spectrosc. Relat. Phenom. **141**, 121 (2004).
[12] Y. Hikosaka *et al.*, J. Phys. B (to be published).
[13] H. Ågren *et al.*, J. Electron Spectrosc. Relat. Phenom. **14**, 27 (1978).
[14] T. Wahi *et al.*, Ann. Phys. (N.Y.) **19**, 59 (1994).
[15] A. Albiez, M. Thoma, W. Weber, and W. Mehlhorn, Z. Phys. D **16**, 97 (1990).
[16] D. Chattarji, W. Mehlhorn, and V. Schmidt, J. Electron Spectrosc. Relat. Phenom. **13**, 97 (1978).
[17] T. Mukoyama and K. Taniguchi, Phys. Rev. **36**, 693 (1987).
[18] S. Svensson, N. Mårtensson, and U. Gelius, Phys. Rev. Lett. **58**, 2639 (1987).
[19] S. Svensson *et al.*, J. Electron Spectrosc. Relat. Phenom. **47**, 327 (1988).
[20] V. Carravetta, J. Phys. B **21**, 1777 (1988).
[21] V. G. Yarzhemsky, M. Y. Amusia, and L. V. Chernysheva, J. Electron Spectrosc. Relat. Phenom. **127**, 153 (2002).
[22] U. Fano, Phys. Rev. **124**, 1866 (1961).
[23] J. Jimenez-Mier, J. Quant. Spectrosc. Radiat. Transfer **51**, 741 (1994).
[24] L. Avaldi *et al.*, J. Phys. B **30**, 5197 (1997).
[25] U. Hergenhahn *et al.*, J. Phys. Chem. A **105**, 5704 (2001).